The measurement of rain kinetic energy and rain intensity using an acoustic disdrometer

2012 Meas. Sci. Technol. 23 015801

(http://iopscience.iop.org/0957-0233/23/1/015801)

Meas. Sci. Technol. **23** (2012) 015801 (9pp) doi:10.1088/0957-0233/23/1/015801

The measurement of rain kinetic energy and rain intensity using an acoustic disdrometer

P Winder and K S Paulson

Department of Engineering, University of Hull, Hull HU6 7RX, UK

E-mail: philipwinder@gmail.com

Received 12 September 2011, in final form 30 October 2011
Published 5 December 2011
Online at stacks.iop.org/MST/23/015801

Abstract
Microwave engineers and geomorphologists require rainfall data with a much greater temporal resolution and a better representation of the numbers of large raindrops than is available from current commercial instruments. This paper describes an acoustic instrument that determines rain parameters from the sound of raindrops falling into a tank of water. There is a direct relationship between the kinetic energy (KE) of a raindrop and the acoustic energy that it creates upon impact. Rain KE flux density is estimated from measurements of the sound field in the tank, and these have been compared to measurements from a co-sited commercial disdrometer. Eight months of data have been collected in the eastern UK. Comparisons of rain KE estimated by the two instruments are presented and links between the KE and rainfall intensity are discussed. The sampling errors of the two instruments are analysed to show that the acoustic instrument can produce rain KE measurements with a 1 s integration time with sampling uncertainty of the same size as commercial instruments using a 1 min integration time.

Keywords: rain, disdrometer, acoustic, rain rate, kinetic energy

1. Introduction

Rain disdrometers are instruments that determine the distribution of drop sizes present in rain, e.g. the Joss–Waldvogel (JW) impact disdrometer or the Thies–Clima laser precipitation monitor (LPM). Typically, they measure the parameters of individual drops as they impact on, or fall through, a horizontal catchment area or estimate the drop size distribution (DSD) from empirical relationships. The JW disdrometer deduces drop sizes from drop momentum, while the Thies–Clima LPM measures the amount of light scattered out of a laser beam. The near simultaneous arrival of two or more drops at the catchment leads to erroneous measurements, and so these instruments have small catchments of 50 and 25 cm^2, respectively. This limits the instruments to long integration times, typically 1 min, and even then the sampling statistics are poor for the large drop tail of the size distribution. The long integration times and poor estimates for the incidence of large drops mean that the data from these instruments are inadequate for some applications.

Several applications exist where the effects of rain are highly nonlinear with respect to the drop size and which are sensitive to sub-minute rain variation, for example, erosion and radio communications. The scatter of microwaves by rain is important in telecommunications and radar meteorology, COST 210 (1991). At microwave frequencies this is a Rayleigh scattering process where the scatter from a raindrop is proportional to its diameter to the sixth power and so radar reflectivity and microwave specific attenuation are very sensitive to the numbers of large drops. Furthermore, the performance of a microwave telecommunications link is measured using metrics that depend upon the second-to-second variation in bit error rate (BER). The BER is related to the total rain fade which is approximately determined by all the raindrops in the first Fresnel zone of the link. This volume is typically of the order of metres across and often only a few hundred metres long. Consequently, the simulation of microwave channels requires high temporal resolution DSD measurements with accurate large drop tails. Similarly, erosion processes are sensitive to rapid rain variations that

are highly nonlinear with respect to drop size (van Dijk *et al* 2002). Erosivity is a combined function of the rain intensity (RI) and of its velocity, so rain KE flux is often cited as a primary indicator (e.g. Brodie and Rosewell 2007, Salles and Poesen 2000). A large proportion of the KE is carried by the small proportion of larger drops.

An alternative approach to that used by disdrometers currently on the market is to determine rain parameters from the sound generated from raindrop impacts upon a body of water (e.g. Nystuen 1987, 2001, Oguz and Prosperetti 1991, Nystuen *et al* 1993, Ma *et al* 2005). The acoustic signal produced by a drop impact can be as short as 10 μs and so potentially large numbers of individual impacts can be measured over a short time interval. This allows large catchment areas and short integration times, e.g. 1 s or shorter. Some rain parameters can be deduced from the total sound field, which is much simpler than identifying individual impacts, and this allows even larger catchments and higher temporal resolution. For total sound field measurements these instruments are limited by the quality of amplifying equipment, the number of listening devices and the power in extraneous noise.

All known total sound field rain measurements have been derived from acoustic rain gauges (ARGs) designed for use at sea, where standard instruments are not appropriate. These ARGs are suspended between 20 and 2000 m below the water surface and measure the sound of rain falling on an effective catchment area between 60 and 10 000 m across. For the shallowest ARG this is six orders of magnitude larger than the JW or LPM disdrometer catchment and could yield measurements with considerably shorter integration times. The limitations of the method arise from rain inhomogeneity over the catchment, with difficulties in distinguishing the sound produced by drops in different size ranges in the total sound field and filtering out other sound sources, e.g. waves, wind, ships and animals.

In this paper, we describe the development of an acoustic water tank disdrometer (AWTD) for use on land. The term disdrometer is used to signify the subsequent estimation of the DSD, which is discussed in a later paper. The measurement of the total sound field in a water tank removes the majority of noise contamination sources present in marine measurements. This paper examines the measurement of RI and KE from the total sound field. A later paper will report the measurement of DSD parameters from examination of the acoustic signal produced by individual drop impacts.

In section 2, we summarize the processes that convert energy in a raindrop to acoustic energy and the properties of acoustic signals generated by the impact of a water drop on a liquid surface. Section 3 describes the design and construction of the AWTD, both the physical properties of the tank and the signal processing electronics. Section 4 develops algorithms for estimating rain parameters from tank measurements, while section 5 compares tank-derived parameters from those derived from measurements of a co-sited LPM. Section 6 provides some conclusions and discusses future work.

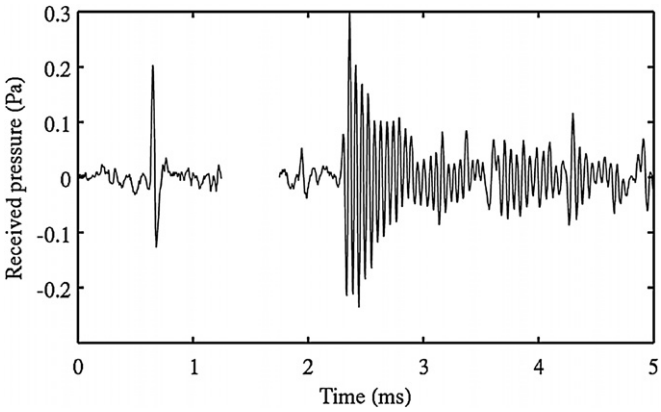

Figure 1. A typical measured droplet impact and bubble signal using the AWTD in laboratory conditions.

2. Background

Since 1959 several studies have shown that there are three main sources of sound generated by a water drop falling on a water surface, each with different temporal character and frequency content (Medwin *et al* 1992). The impact of raindrops on the water surface generates a sharp initial pressure rise corresponding to radiated sound of short duration (between 10 and 40 μs) and a damped pressure wave with predominantly low frequency content (below 600 Hz) associated with a near field hydrodynamic effect. Raindrops also generate strongly radiating air bubbles that are formed from several tens to hundreds of ms after the impact. These bubbles oscillate and radiate sound with frequencies of 10–50 kHz for up to 10 ms before reaching a state of equilibrium. In laboratory studies using a 26 m long vertical utility shaft and an anechoic water tank (a 1.5 m high and 1.5 m diameter cylindrical redwood barrel with a lining of redwood wedges), Medwin *et al* (1992) have carried out a comprehensive analysis of the acoustic signatures for drops of different sizes and found that the relative proportions of impact and bubble noise vary with drop size. Drops below 0.7 mm in diameter were not heard. Drops with diameters in the range 0.8–1.1 mm (associated with drizzle) cause an impulse lasting for less than 10 μs and loud bubble noise across the frequency range 12–21 kHz. Typically, drops with diameters in the range 1.1–2.2 mm cause loud impact noise but do not create bubbles. Large drops with diameters above 2.2 mm cause very loud impact and bubble noise across the frequency range 1–50 kHz, although not all large drops create bubbles. Medwin *et al* (1992) derived an empirical relationship between the peak frequency of the bubble noise in the range 12–21 kHz and the raindrop volume. Mani and Pillai (2004) have shown that the acoustic signature of the pressure wave associated with raindrop impact on a water surface can be used for drop size measurement.

Figure 1 illustrates an acoustic signal measured by a hydrophone, generated by the impact of a raindrop on a water surface. The signal around 0.7 ms is the impact pulse while the damped ringing from 2 ms onwards is due to bubble oscillation. For this illustration, the time interval between impact and bubble noise has been reduced for clarity. Typical durations are between 1 and 500 ms.

The bubble noise is a serious problem when attempting to estimate rain parameters from the acoustic signal generated by rain falling into water. It increases the duration of the acoustic signal generated by a drop impact from as short as 10 μs to as long as 0.5 s. This greatly reduces the rate at which individual drop signals can be generated before they overlap. Furthermore, the bubble noise is often of higher amplitude than the impact pulse. Potentially this can lead to bubble noise being interpreted as multiple drop impacts. The bubble noise produced by a specific drop is also highly variable and depends upon parameters we cannot measure, such as the impact angle and the internal hydrodynamics of the drop, e.g. see Medwin *et al* (1990).

Regular entrainment (Franz 1959, Pumphrey and Crum 1989) refers to the process where a bubble is created when a droplet impacts on the surface of a liquid, usually water. Several studies developed the mechanics of entrainment (Prosperetti and Oguz 1993) and found that there are several scenarios when entrainment can occur. Regular entrainment occurs when a crater is formed in the water after an impact. As the liquid returns to its equilibrium, and since the drop is still forcing the surface of the liquid downwards, the sides of the crater can collapse or 'pinch-off' due to a travelling capillary wave. The resulting void at the bottom part of the crater forms a bubble. Irregular-shaped raindrops can also produce entrained bubbles. Raindrop shape is determined by the internal hydrodynamics and the air drag. Large drops are approximately oblate spheroids and very large drops become concave at the bottom. When a large drop impacts the water surface, the preceding air is forced into the water and develops into an 'azimuthal necklace' (Thoroddsen *et al* 2003). Surface tension then breaks up the necklace into a ring of stable bubbles. The third type of entrainment is formed when, after an initial large impact, further smaller droplets are ejected from the impact site and create their own bubbles via the first two entrainment processes. This can be due to funnel formation and separation from a crater collapse or from a crown formation, ejecting droplets into the air when a crater is formed with a very large energy impact. Irrespective of the type of entrainment, the resultant bubble will experience the comparatively large pressure of being underwater. This will contract the bubble until the growing internal pressure slows the contraction to a halt. The bubble will then expand again, oscillating and radiating sound until the two pressures reach equilibrium. Because the entrained air is not spherical, there will also be spherical harmonic oscillations until it regains spherical equilibrium.

The effect of wind has been investigated by Medwin *et al* (1990). Falling raindrops are advected horizontally by the wind resulting in oblique incidence on the water surface. As a consequence, the probability of bubble production is altered and the amount of energy in the impact pulse changes. They found that with an increasing wind speed, the resultant spectrum of the rain induced total sound field alters. As the angle of incidence increases, less bubbles are created and their contribution to the spectra becomes weaker and changes to higher frequencies. At the same time, the contribution to the spectrum from the broadband impact signal becomes stronger.

Many researchers have reported that the acoustic spectra of the total sound field are produced by natural rain falling into water (e.g. Lavile *et al* 1991, Medwin *et al* 1992, Nystuen *et al* 1993, Pumphrey and Crum 1989). These studies found that most rain events yielded a spectral peak at around 14–16 kHz, principally generated by entrainment. Medwin *et al* (1992) also showed that bubbles with a range of sizes created sound between 1 and 50 kHz. The impact signal is impulse-like in time and the corresponding spectrum is broadband in nature, although it reduces as the frequency increases due to the finite pulse duration.

Originally it was planned to suppress all bubble production by the addition of a surfactant, in order to derive relationships that were independent of bubble noise. Pumphrey and Crum (1989) stated that if the water surface tension was reduced below 30 dyn cm^{-1} (30 mN m^{-1}), the production of entrained bubbles was eliminated. Experimentally it was found that the addition of surfactants to decrease the surface tension promotes the formation of bubbles on the surface of the water. These bubbles would then cushion subsequent drops and eventually burst, resulting in another high amplitude signal. It was found that a 1 cm thick layer of cooking oil floating on the water surface suppressed bubble production since the viscosity of the oil reduced the size of crater formation to the point where it would not pinch off and create a bubble. This has been confirmed by recent work by Deng *et al* (2007), who formulated the idea of a capillary number, the ratio between viscosity and surface tension. However, oil was not suitable for a rain measurement instrument as heavy rain lead to pools of water on the oil surface, and the oil was not stable for long periods due to the growth of algae and bacteria.

As we have not found a way of suppressing bubble noise, rain parameter estimation algorithms need to be consistent with the stochastic bubble noise production process.

3. The acoustic water tank disdrometer

Data were collected in a water-filled, cylindrical plastic tank, with a cross-sectional area of 0.38 m^2 and a depth of 0.5 m. The tank was lined with a combination of natural rubber and foam to form a semi-anechoic lining.

The purpose of the lining is to reduce the duration of the impulse response for each drop impact. In subsequent experiments where individual drop impacts are identified, it is important to minimize the reflection of acoustic waves by the tank walls as these waves could be interpreted as new drop impacts. One measure of the absorption within an anechoic lining is the acoustic loss factor, which is the ratio of reflected to incident acoustic power. The loss factor accounts for all methods of loss, e.g. elastic and frictional. Using an impacting drop as an acoustic source, a loss factor of approximately 0.1 was obtained for the rubber–foam lining. This value is in accordance with the work of Ouis (2005), where the effectiveness of the anechoic lining, and hence the loss factor, is halved due to the lack of damping at the water–air interface.

Four SRD HS/150 omnidirectional hydrophones were fastened to the inside, bottom (i.e. 0.5 m deep) of the tank,

Figure 2. An image of the experimental setup.

100 mm from the centre, located in north, south, east and west positions. Each hydrophone is connected to a proprietary amplifier designed to optimize the dynamic range. The noise floor for a single hydrophone in the presence of all noise sources was measured to be 0.11 Pa, which yielded a dynamic range of 60 dB. The amplified signal is sampled at 200 kHz, with 24-bit resolution, using a PC hosted NI-4462 data acquisition card. The measurements are archived by the PC.

A Thies–Clima LPM is sited within 0.5 m of the tank edge and at the same level as the water surface. Both instruments are installed in a suburban garden in Hull, UK (53.76735°N, 0.366345°W). The instruments are approximately 10 m from the southern aspect of a two-storey house and there are trees over 20 m tall, approximately 50 m from the instruments. Although the situation is far from ideal for accurate rain parameter measurements, due to disturbance of the wind field by the buildings and trees, we are interested in comparing parameters estimated from the LPM and the acoustic measurements made in the tank. It is reasonable to expect the two instruments to experience the same rain parameters.

The LPM is operated in event mode where the diameter and fall speed of each drop is recorded. This allows DSD and related parameters to be calculated with a range of integration periods. A large amount of data is produced and this will begin to saturate the serial data connection at rain intensities in excess of 100 mm h^{-1}. However, rain at this intensity typically occurs for only 1 or 2 min a year in Hull.

An image depicting this setup is shown in figure 2. Steiner and Smith (2000) and Prosperetti and Oguz (1993) have shown that some of the KE of the raindrops landing on a water surface is transformed into acoustic energy, in a fraction of a second, by a range of processes. The impact pulse and entrained bubble noise, due to the primary impact and splash products, carry the bulk of the energy while smaller amounts generate eddies near the impact, surface waves, atmospheric sound and splash products that fall outside the tank. In this paper, we test the hypothesis that the acoustic energy measured in the tank over a second or longer is proportional to the KE carried by the raindrops falling onto the water surface. This hypothesis was tested by comparing 1 min raindrop KE accumulations estimated using the velocities and drop sizes measured by the LPM, with the total acoustic energy measured by average of the four tank hydrophones.

4. Comparison of instrument measurements

Over a period of eight months beginning in October 2009, rain events were observed with simultaneous recording of the sound field in the water tank at the four hydrophones and the drops arriving at the LPM. The objective was to determine which rain parameters, at what temporal resolution, could be derived from the acoustic measurements. Both instruments yield measurements affected by a range of systematic and random errors. When comparing measurements, it is important to understand what differences are significant. The largest uncertainty is introduced by the relatively small sample volume of the LPM, i.e. the drops recorded by the LPM are unlikely to be representative of the DSD in the atmosphere above the instruments. In the paragraphs below, we derive expressions for the uncertainty in measured rain parameters in terms of the instrument sample volumes.

4.1. Sampling errors in measured rain parameters

Rain measurements typically derive rain parameters from the raindrops in a sample volume of atmosphere, e.g. meteorological radar, or the raindrops that cross a horizontal catchment area in an interval of time, e.g. a rain gauge or disdrometer. The raindrops in the sample will have different sizes and relative positions each time a measurement is performed, even if the notional rain parameter, e.g. RI or rain KE, is constant. This yields a temporal fluctuation in the measured parameter around the notional value and a distribution of measured values, characterized by a variance.

The numbers and relative positions of raindrops in the atmosphere are determined by very complex processes including coalescence and break-up, along with evaporation and turbulent inertial sorting. Although this leads to some clustering, drop arrivals at a catchment are often modelled as a Poisson process. The distribution of drops over some small diameter range, i.e. $[D, D + \mathrm{d}D]$, can be modelled as Poisson as drops of a particular size are likely to have been produced by different, and uncorrelated, break-up events. The same arguments hold for the arrival of raindrops at an instrument catchment area. This has been experimentally verified by Joss and Waldvogel (1969). If we assume that the arrival of drops in a small size interval is a Poisson process (Onof *et al* 2000), this allows the calculation of the variation in rain parameters derived from DSD measurements over a range of integration intervals. The Poisson distribution is discrete and has the property that the mean is equal to the variance.

4.2. Sample errors in catchment rain measurements

Instruments such as rain gauges and disdrometers measure rain parameters from the raindrops that cross a catchment area A in an integration time T. These instruments can be thought of as sampling a prism of atmosphere above the instrument with cross-section A and height $V(D)T$, where $V(D)$ is the fall speed of drops of diameter D. The sample volume is larger for larger raindrops with more rapid fall speed. This is an advantage for disdrometers as a higher proportion of large drops are measured, compared to a volume sampling instrument, yielding better sampling statistics at the large diameter tail of the DSD. If horizontal wind is present, the sample prisms are no longer perpendicular to A, but have the same volume.

Consider a notional rain event with a uniform mean RI of $\bar{R}$ mm h^{-1}. If the sizes of raindrops are Marshall–Palmer distributed (Marshall and Palmer 1948), then the mean number of drops per unit volume, in the diameter interval $[D, D+\mathrm{d}D]$, is given by $N(D)\,\mathrm{d}D = \Lambda_0\,\mathrm{e}^{-\lambda D}\,\mathrm{d}D$, where Λ_0 is a constant and $\lambda(\bar{R})$ is a function of the mean RI. The mean number of drops in each size range, measured by the disdrometer, is

$$N_{\mathrm{disd}}(D)\,\mathrm{d}D = AT\ V(D)N(D)\,\mathrm{d}D, \tag{1}$$

where $N_{\mathrm{disd}}(D)$ is the observed DSD. Due to the Poisson assumption, the variance of this measurement is

$$\begin{aligned}\mathrm{Var}(N_{\mathrm{disd}}(D)\,\mathrm{d}D) &= N_{\mathrm{disd}}(D)\,\mathrm{d}D \\ &= AT\ V(D)N(D)\,\mathrm{d}D.\end{aligned} \tag{2}$$

The best estimate of $N(D)\,\mathrm{d}D$ derived from the disdrometer measurement is

$$N(D)\,\mathrm{d}D \cong \frac{N_{\mathrm{disd}}(D)\,\mathrm{d}D}{ATV(D)} \pm \sqrt{\frac{N(D)\,\mathrm{d}D}{ATV(D)}}. \tag{3}$$

It is clear that diameter ranges with small numbers of measured drops yield poor estimates of the number density of these drops in the atmosphere, e.g. a bin with ten measured drops yields an atmospheric number density with a 30% relative error.

Note that from (3) the variance is inversely proportional to the catchment area of the instrument and the measurement integration time. The AWTD has a catchment area approximately 85 times larger than the LPM and so would yield RI estimates with the same standard error using an integration time 85 times shorter.

4.3. Comparison of tank and LPM rain KE intensity

Measurement of acoustic energy allows estimation of the rain KE flux density, i.e. the rate that raindrops falling through a horizontal surface transport KE. The KE intensity due to drops of diameter D is

$$I_{\mathrm{KE}}(D) = \frac{1}{AT}\mathrm{KE}(D)N_{\mathrm{disd}}(D)\,\mathrm{d}D, \tag{4}$$

where $\mathrm{KE}(D) = \frac{1}{2}\rho\,\mathrm{Vol}(D)V^2(D)$ is the KE of a drop of volume $\mathrm{Vol}(D)$ and ρ is the density of water. The variance in the KE flux density estimate is

$$\mathrm{Var}(I_{\mathrm{KE}}) = \frac{1}{(AT)^2}\int_0^\infty \mathrm{KE}^2(D)N_{\mathrm{disd}}(D)\,\mathrm{d}D. \tag{5}$$

Writing (5) in terms of the atmospheric DSD, as in (3), similarly concludes that the variance due to sampling error is inversely proportional to both catchment area and integration time.

The LPM estimates the vertical component of drop velocity from the amount of light scattered out of a horizontal beam and the duration of the scattering. Horizontal movement is not detected. The KE of drops moving horizontally with the wind have higher KE than drops falling vertically. If drops are moving with a wind speed W, then the KE is increased to

$$\mathrm{KE}(D, W) = \tfrac{1}{2}\rho\,\mathrm{Vol}(D)(V^2(D) + W^2). \tag{6}$$

For moderate wind speeds around 5 m s^{-1}, this doubles the KE of drops of diameter 1.3 mm and greatly increases the KE of smaller drops. This increased KE will be measured by the tank disdrometer, but not detected by the LPM. Furthermore, Medwin *et al* (1990) have shown that the acoustic intensity will alter with a drop's angle of incidence, caused by a decreasing probability that a drop will cause entrainment.

4.4. Rain KE flux

Figure 3 is the scatter plot of these two quantities with error bars indicating the standard deviations of LPM-derived rain KE flux density calculated using (5) and (6). All rain events over the eight months observation period were used except for those the LPM determined were hail, snow or sleet. A total of 25 h of rain was observed with a maximum rain rate of 40 mm h^{-1}. This is typical for the experiment location.

The acoustic intensity measurements are first averaged over all four hydrophones, and the integrated over time to obtain a measure of the acoustic flux density. The data need to be adjusted at low rain intensities to remove the noise inherent in the measurement electronics. As the system noise and rain-generated signal are uncorrelated, the total measured acoustic energy is the sum of noise plus signal energies. Hence, the resultant acoustic pressure measurement is translated to yield zero acoustic intensity at zero KE.

The KE of falling drops needs to be corrected for horizontal movement with the wind. Even for low wind speeds of several metres per second, a large proportion of raindrops would be moving horizontally faster than they are falling. Therefore, the KE derived from LPM measurements is expected to be an underestimate. This underestimation will be more significant at lower rain rates where more drop KE is due to horizontal movement. For this reason the points corresponding to low energy flux densities deviate further from the regression line than due to sampling errors alone.

Temperature affects the speed of sound within the water, but the received acoustic intensity does not change. Hence, results will remain valid so long as the tank and rain are not frozen.

A linear fit to the scatter plot (cf figure 3) is plausible. Using the least-squares regression (LSR) method the following parameters were found to fit KE to the acoustic intensity, AI:

$$\mathrm{KE} = 77.6 \times 10^{-3} \times \mathrm{AI}. \tag{7}$$

A Pearson correlation coefficient of 0.92 was found when using the log parameters as illustrated in figure 3. This compares

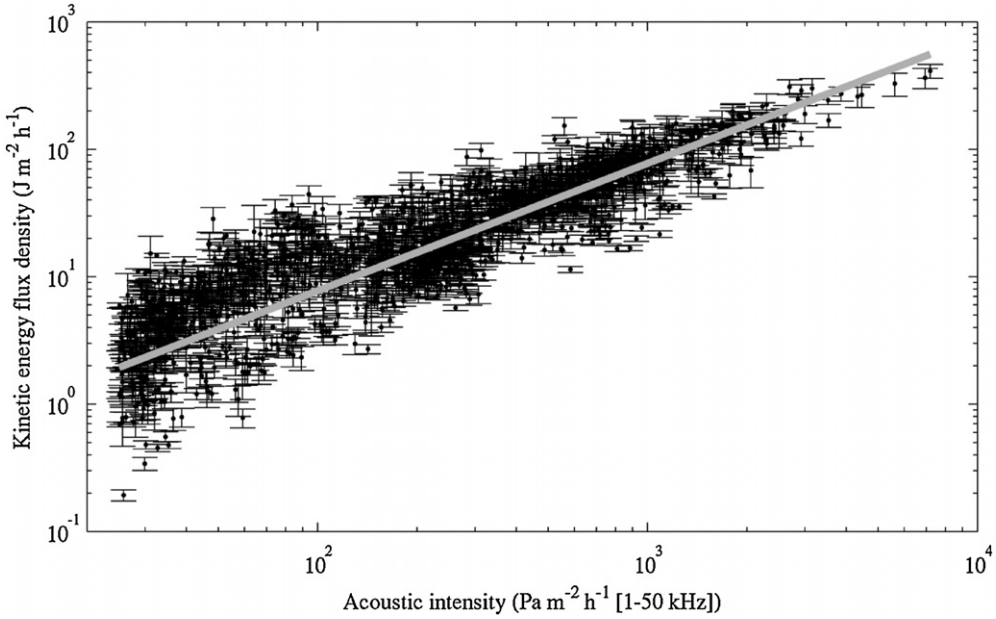

Figure 3. Comparison of the rainfall of the KE flux density measurement with total acoustic energy integrated over 1 min. The error bars indicate uncertainty due to LPM sampling errors. The grey line represents the least-squares best fit of the data. (Acoustic units have been left in pascals to emphasize the acoustic nature of the data. This is proportional to J m^2 h^{-1}.)

well to the correlation coefficients of Nystuen (2001), who found values between 0.79 and 0.94 for various combinations of disdrometers.

From equation (6) it can be seen that the wind speed greatly affects the KE, and hence the acoustic intensity. This manifests in the data by increasing the variance since no discrimination between event wind speeds has been made. The remaining variance can be attributed to the random nature of DSD parameters (see equation (2)).

4.5. Rain intensity

A similar process can be performed for RI estimated using the LPM (see figure 4). Generally, power-law relationships are used to link RI with KE, e.g. see Salles *et al* (2002). As KE has been shown to be proportional to AI, a power-law relationship is expected between RI and AI. Salles *et al* suggest KE $\propto$ RI$^{\beta}$, where $1.06 \leqslant \beta \leqslant 1.35$. The exponent depends upon the assumed form of DSD. This suggests a power-law relationship RI $\propto$ AI$^{1/\beta}$. RI is not affected by the horizontal movement of raindrops although the KE is increased. Therefore, more spread is expected when comparing RI to AI. Figure 3 is a scatter plot of RI against AI. The LSR best fit of the log parameters indicates a power-law exponent of 0.68, which considering the effect of the wind is consistent with the results of Salles,

$$\mathrm{RI} = 60 \times 10^{-3} \times \mathrm{AI}^{0.68}. \tag{8}$$

The Pearson correlation coefficient of the variables log(AI) and log(RI) is estimated to be 0.81. This is lower than the coefficient for KE, due to uncertainties introduced by wind and DSD variations (e.g. inability to hear smaller drops), but still reasonable for rain measurements.

4.6. The effect of wind on KE flux density measurement

From equation (6), it was established that the LPM does not measure the horizontal component of the velocity due to wind, and hence does not truly represent the KE flux density within a rainstorm. To compensate, an anemometer was placed at the LPM site from 13 December 2009.

Figure 5 shows the compensated LPM KE reading after accounting for a horizontal offset caused by wind. Since the AWTD assumes that the KE is proportional to the acoustic pressure, the compensated LPM KE should now correlate better with the AWTD. This would manifest as an improved Pearson correlation coefficient.

The recorded Pearson correlation coefficient of this data was 0.89, which is a slight deterioration of the original correlation coefficient of 0.92. It is suspected that this is due to the comparative lack of data, which is approximately one third of the size of the LPM/AWTD data. Over a further period of time, it is expected that the correlation coefficient will exceed the noncompensated data by a small amount.

The highest average wind speeds within the data are shown as stars in figure 4. These events, which have an average velocity above 1.5 m s^{-1}, have a standard deviation that is 1.5 times greater than the overall deviation and an above average skew. However, the majority of these data are for low rain rates, i.e. an acoustic intensity of 103 Pa m^{-2} h^{-1} corresponds to a RI of approximately 5 mm h^{-1}. The LPM has been shown to exhibit systematic errors depending on wind direction and strength (Brawn 2009), especially at low rain rates. At rain rates above 2 mm h^{-1}, the agreement with the best fit is good, even for the high wind speed events (the three right-most stars).

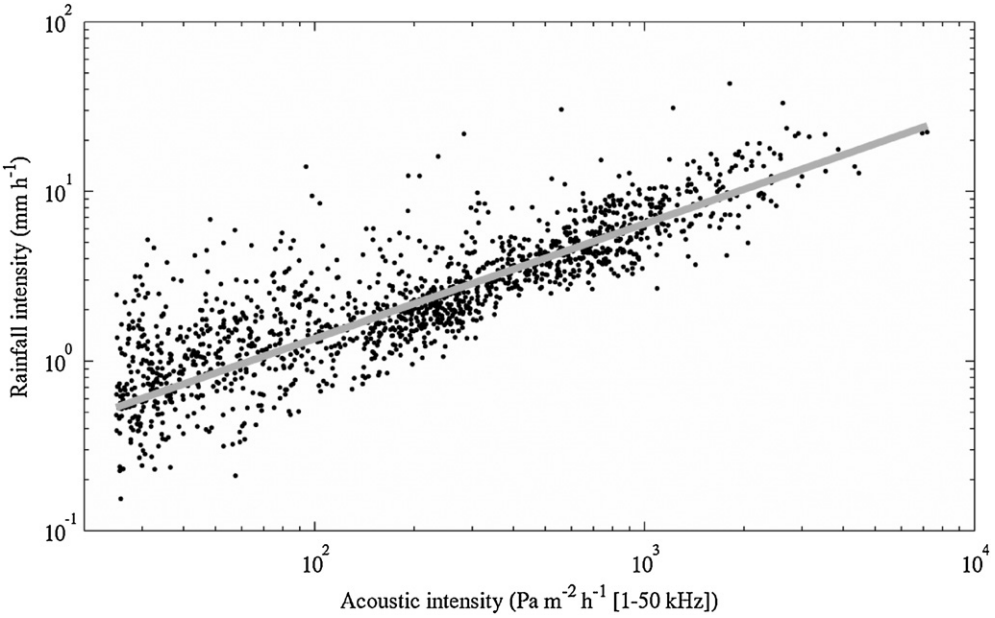

Figure 4. Comparison of LPMs RI measurement with total acoustic energy integrated over 1 min. The grey line represents the least-squares best fit of the data.

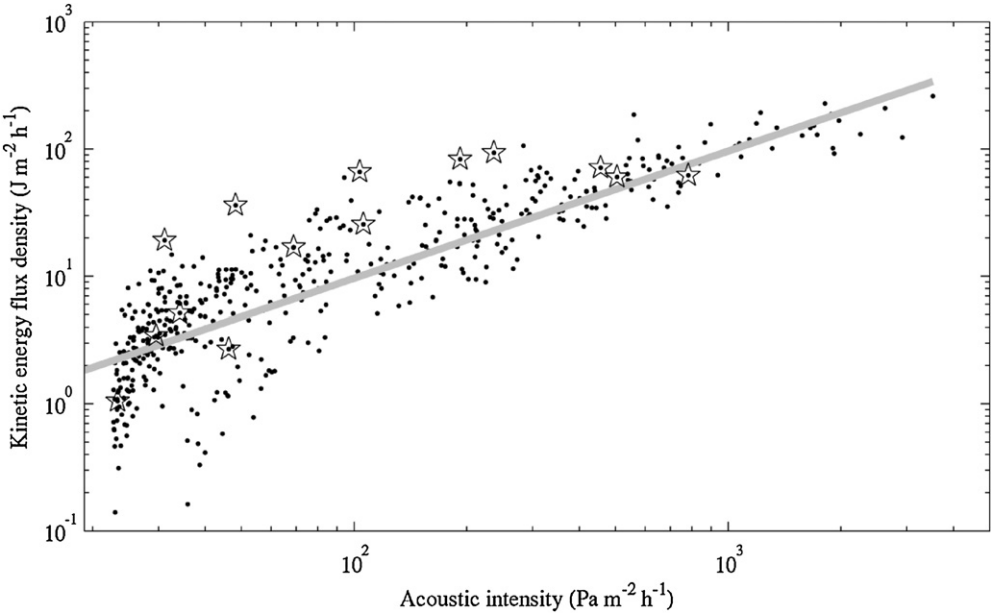

Figure 5. The new KE–AWTD relationship after compensating for the lack of a horizontal wind reading from LPM. Stars indicate the data recorded with the highest average wind speeds.

5. Discussion

As mentioned in section 4.4, a relationship exists between the KE of the impacting drops and the energy in the sound field. Although the power can be calculated using the entire bandwidth of the measurement equipment, i.e. 1–50 kHz, other authors suggest that power in narrow frequency ranges is sufficient to characterize rain parameters and may be less susceptible to noise. Nystuen (2001) suggests using 2.8 kHz for the KE and 1.5 kHz for the RI. Ma *et al* (2005) used the energy at 5 kHz, indicating that the optimal frequency is dependent on operating conditions. However, it is our hypothesis that a fixed proportion of the KE of the incident drops is transformed into acoustic energy, for a wide range of rain conditions. As the production of bubble noise depends upon drop diameter and many other parameters, it is expected that acoustic energy in particular frequency ranges will be dependent upon DSD and operational conditions. Therefore, we prefer the use of the entire impact and bubble spectra to estimate the KE.

Figures 6 and 7 illustrate KE and RI time series for an example rain event recorded on 1 November 2009 at 09:27

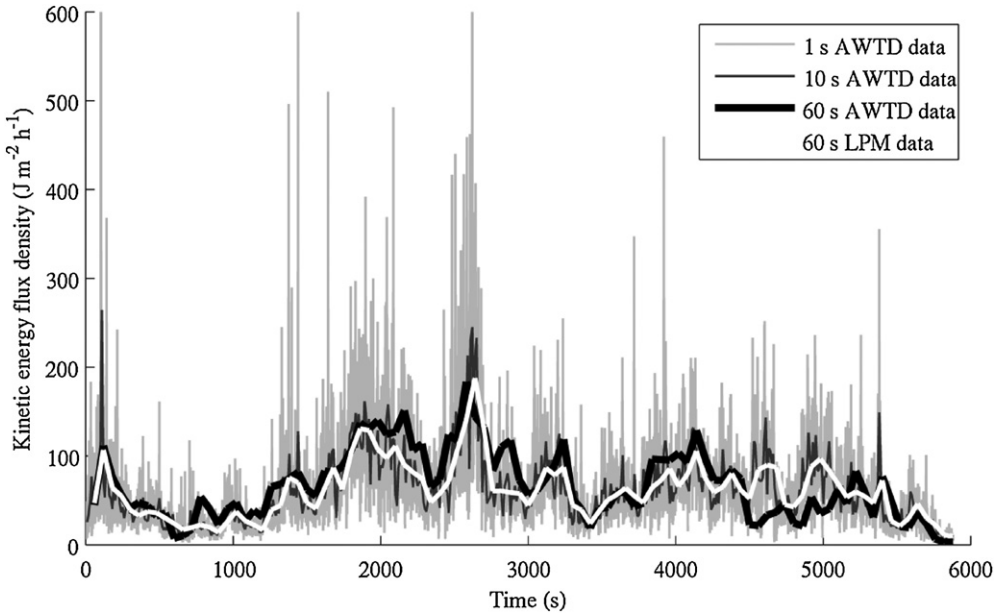

Figure 6. Typical kinetic energy data. The AWTD data at 60, 10 and 1 s integration times (black/grey) are compared to LPM measurements at a 60 s integration time (white).

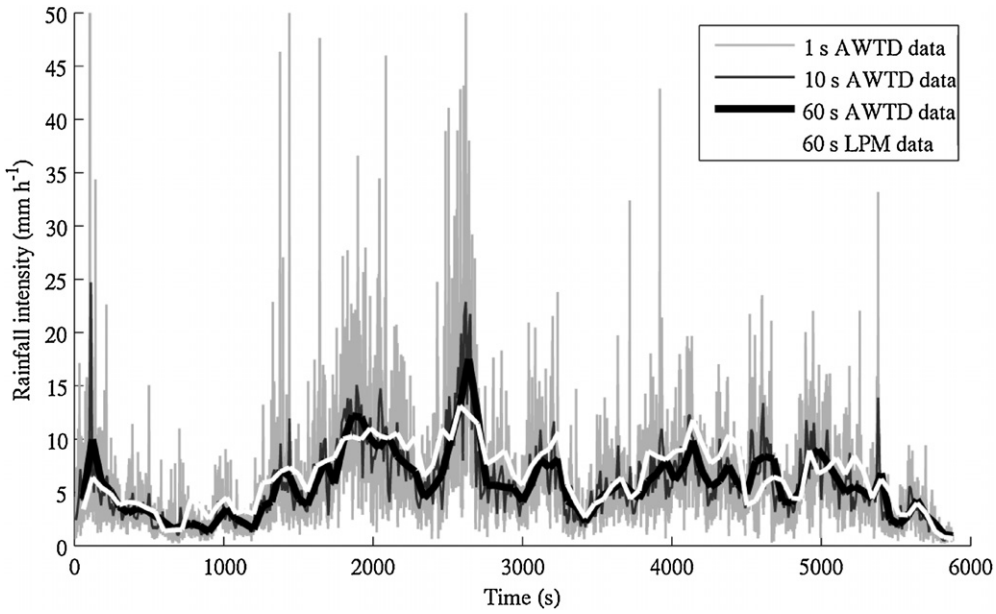

Figure 7. Typical rainfall intensity data. The AWTD data at 60, 10 and 1 s integration times (black/grey) are compared to LPM measurements at a 60 s integration time (white).

with RIs between 5 and 13 mm h^{-1} (cf figure 7), calculated using a 1 min integration time. For both graphs KE and RI are measured using the LPM and estimated using the AWTD and empirical relations (7) and (8). These show broad agreement with differences due to the separation of catchment areas (approximately 1 m between instruments) and volume sampling uncertainties. Nystuen (2001) measures the relative performance of different disdrometers by the means of a Pearson correlation coefficient. The coefficients range from 0.79 to 0.94 indicating that both the KE and RI conversions perform at least as well as other disdrometers.

Section 4 established that the AWTD could provide rain parameters with an integration time as short as 1 s, with the same sampling errors as the LPM with a 1 min integration time, due to its much larger catchment area. Figures 5 and 6 also illustrate AWTD data has been used to estimate these parameters with an integration time of 10 s and 1 s, and these have been compared with 1 min integration time LPM results.

These results illustrate the variation that is not represented in 1 min data. At 1 s resolution, rain intensities that are five times the 1 min average are present. These variations are vital for the understanding of erosion and to engineer fade mitigation techniques for short microwave links.

6. Conclusions

A rain measurement instrument based on listening to raindrops falling into a tank of water has been designed and built. Eight months of rain data have been collected and empirical relationships between the energy in the acoustic sound field within the tank and rain parameters such as rain intensity (RI) and kinetic energy (KE) have been established. Comparing RI and KE measured by a commercial instrument with those derived from acoustic water tank disdrometer measurements, these correlate as well as compare between the pairs of commercial instruments (Nystuen 2001). Furthermore, the new acoustic instrument has been empirically shown to be able to provide measurements with an integration time as short as 1 s. Time series of 1 s variation in rain parameters have shown a factor of five variations around 1 min averages. However, further improvements could be made by a dissection of the spectral components (e.g. not including parts of the spectra that are created by entrainment or investigating the use of principal component analysis).

References

Brawn D 2009 An elementary estimation of gamma parameters and the analysis of disdrometer data *PhD Thesis* Department of Mathematical Sciences, University of Essex

Brodie I and Rosewell C 2007 Theoretical relationships between rainfall intensity and kinetic energy variants associated with stormwater particle washoff *J. Hydrol.* **340** 40–7

COST 210 Management Committee 1991 Influence of the atmosphere on interference between radio communications systems at frequencies above 1 GHz *COST 210* (Brussels: European Commission)

Deng Q, Anilkumar A V and Wang T G 2007 The role of viscosity and surface tension in bubble entrapment during drop impact onto a deep liquid pool *J. Fluid Mech.* **578** 119–38

Franz G J 1959 Splashes as a source of sound in liquids *J. Acoust. Soc. Am.* **31** 1080–96

Joss J and Waldvogel A 1969 Raindrop size distribution and sampling size errors *J. Atmos. Sci.* **26** 566–9

Lavile F, Abbott G D and Miller M J 1991 Underwater sound generation by rainfall *J. Acoust. Soc. Am.* **89** 715–21

Ma B B, Nystuen J A and Lien R J 2005 Prediction of underwater sound levels from rain and wind *J. Acoust. Soc. Am.* **117** 3555–65

Mani T K and Pillai P R S 2004 Drop parameter estimation from underwater noise produced by raindrop impact *Acoust. Res. Lett. Online* **5** 118–24

Marshall J S and Palmer W M 1948 The distribution of raindrops with size *J. Atmos. Sci.* **5** 165–6

Medwin H, Kurgan A and Nystuen J A 1990 Impact and bubble sound from raindrops at normal and oblique incidence *J. Acoust. Soc. Am.* **88** 413–8

Medwin H, Nystuen J A, Jacobus P W and Ostwald L H 1992 The anatomy of underwater rain noise *J. Acoust. Soc. Am.* **92** 1613–23

Nystuen J A 1987 Rainfall measurements using underwater ambient noise *J. Acoust. Soc. Am.* **79** 972–82

Nystuen J A 2001 Listening to raindrops from underwater: an acoustic disdrometer *J. Atmos. Oceanic Technol.* **18** 1640–57

Nystuen J A, McGlothin C C and Cook M S 1993 The underwater sound generated by heavy rainfall *J. Acoust. Soc. Am.* **93** 3169–77

Oguz H N and Prosperetti A 1991 Numerical calculation of the underwater noise of rain *J. Fluid Mech.* **228** 417–42

Onof C, Chandler R E, Kakou A, Northrop P, Wheater H S and Isham V 2000 Rainfall modelling using Poisson-cluster processes: a review of developments *J. Stoch. Environ. Res. Risk Assess.* **14** 384–411

Ouis D 2005 Modelling the mechanical properties of rubber by means of a five-parameter dispersive model *Proc. Int. Rubber Conf. (Yokohama)*

Prosperetti A and Oguz H N 1993 The impact of drops on liquid surfaces and the underwater noise of rain *Annu. Rev. Fluid Mech.* **25** 577–602

Pumphrey H C and Crum L A 1989 Underwater sound produced by individual drop impacts and rainfall *J. Acoust. Soc. Am.* **85** 1518–26

Salles C and Poesen J 2000 Rain properties controlling soil splash detachment *Hydrol. Processes* **14** 271–82

Salles C, Poesen J and Sempere-Torres D 2002 Kinetic energy of rain and its functional relationship with intensity *J. Hydrol.* **257** 256–70

Steiner M and Smith J A 2000 Reflectivity, rain rate and kinetic energy flux relationships based on raindrop spectra *J. Appl. Meteorol.* **39** 1923–40

Thoroddsen S T, Etoh T G and Takehara K 2003 Air entrapment under an impacting drop *J. Fluid Mech.* **478** 125–34

van Dijk A I J M, Bruijnzeel L A and Rosewell C J 2002 Rainfall intensity-kinetic energy relationships: a critical literature appraisal *J. Hydrol.* **261** 1–23